RSC Advances

PAPER

View Article Online
View Journal | View Issue

Cite this: *RSC Adv.*, 2025, **15**, 46465

Polydopamine-based electrochemical immunosensor for sensitive and selective detection of cotinine

Ohnmar Zaw,[ab] Nang Noon Shean Aye,[b] Jureerut Daduang,[b] Patcharaporn Tippayawat,[b] Patutong Chatchawal,[b] Chavis Srichan,[c] Nichada Jearanaikoon[d] and Pornsuda Maraming *[b]

Tobacco use is a leading cause of preventable disease and death worldwide. Cotinine, the primary metabolite of nicotine, is widely recognized as a reliable biomarker for tobacco exposure. In this study, we developed a sensitive and specific electrochemical biosensor for cotinine detection using polydopamine nanoparticles (PDA NPs) conjugated with anti-cotinine antibodies. Dynamic light scattering and Fourier transform infrared spectroscopy confirmed successful antibody conjugation and nanoparticle functionalization. The optimized biosensor exhibited diffusion-controlled redox behaviour and a linear response across a wide cotinine concentration range (0.1–10 000 ng mL^{-1}), with a detection limit of 0.07 ng mL^{-1}. Differential pulse voltammetry, cyclic voltammetry, and electrochemical impedance spectroscopy validated sensor performance. Recovery analysis in diluted human urine demonstrated good reproducibility. The biosensor also showed high specificity against common interferents and retained over 80% of its signal after six weeks at room temperature. These findings demonstrate the potential of the PDA NPs-based electrochemical immunosensor for rapid, cost-effective, and point-of-care detection of cotinine in biological fluids.

Received 30th July 2025
Accepted 19th November 2025

DOI: 10.1039/d5ra05523g

rsc.li/rsc-advances

1 Introduction

Tobacco use remains a major global health threat, causing over 8 million deaths annually, including 1.2 million from second-hand smoke inhallation.[1] It is a leading risk factor for cardiovascular disease, respiratory illnesses, cancers, and immune-related disorders.[2–4] Tobacco is consumed in many forms, including cigarettes, chewing tobacco, snuff, second-hand smoke, and electronic nicotine delivery systems.[5,6] Despite widespread awareness, tobacco use persists worldwide, highlighting the importance of monitoring tobacco exposure for public health. Cotinine, a key nicotine metabolite, is widely used as a gold-standard biomarker of tobacco exposure. Nicotine is metabolized by cytochrome P450 2A6 (CYP2A6) into a nicotine-delta-iminium ion and then by aldehyde oxidase into cotinine.[7,8] Cotinine has a longer half-life (approximately 20 hours) than nicotine (2–3 hours), allowing detection for 4–5 days. Urine samples were chosen in this study because cotinine concentrations are higher and more stable than those in serum (10–20 ng mL^{-1}) or saliva (10–25 ng mL^{-1}), enabling reliable and non-invasive detection.[9] Urinary cotinine levels can distinguish non-smokers (<10 ng mL^{-1}), passive smokers (11–30 ng mL^{-1}), and active smokers (>500 ng mL^{-1}). These cutoffs aid in clinical and population-level assessment.[10]

Traditional methods for cotinine quantification, such as gas chromatography-mass spectrometry, high-performance liquid chromatography, enzyme-linked immunosorbent assay, and colorimetric assays, offer excellent sensitivity and specificity.[11–15] However, these techniques require complex instrumentation, skilled personnel, long processing times, and are often cost-prohibitive for point-of-care testing (POCT) or large-scale screening applications, especially in low-resource settings. To overcome these limitations, recent research has focused on developing electrochemical biosensors for cotinine detection. These biosensors offer several advantages, such as portability, cost-effectiveness, rapid response time, and ease of integration into POCT devices.[16] The performance of such biosensors is significantly enhanced through the integration of nanomaterials that provide a high surface area, excellent conductivity, and facile functionalization sites for bio-recognition elements.[17–19]

Among various nanomaterials utilized in biosensor development, antibody-functionalized nanoparticles have emerged

[a]*Biomedical Sciences Program, Graduate School, Khon Kaen University, Khon Kaen 40002, Thailand*

[b]*Centre for Research and Development of Medical Diagnostic Laboratories, Faculty of Associated Medical Sciences, Khon Kaen University, Khon Kaen 40002, Thailand. E-mail: pornsma@kku.ac.th*

[c]*Department of Computer Engineering, Faculty of Engineering, Khon Kaen University, Khon Kaen, 40002, Thailand*

[d]*Synchrotron Light Research Institute (Public Organization), Nakhon Ratchasima 30000, Thailand*

as powerful tools for enhancing analytical performance due to their specificity, stability, and signal amplification capabilities. For example, gold nanoparticles (AuNPs) are frequently used because of their high conductivity and strong affinity for thiol- or amine-functionalized antibodies, allowing for stable and oriented conjugation.[20–22] Magnetic nanoparticles enable efficient analyte separation and antibody attachment through surface functionalization, improving biosensor selectivity.[23] Silica nanoparticles offer abundant hydroxyl groups that can be modified for covalent bonding with antibodies, making them suitable for electrochemical biosensors.[24] Carbon-based nanomaterials, including carbon nanotubes and graphene, provide large surface areas and excellent electrical properties, allowing them to serve as robust platforms for antibody conjugation.[25,26]

In many of these studies, the nanoparticle surface is first modified to introduce carboxyl or amine groups before conjugating with the antibody *via* carbodiimide chemistry. Among various nanomaterials explored, polydopamine nanoparticles (PDA NPs) have gained increasing attention due to their unique physicochemical properties.[27] PDA is a mussel-inspired, biocompatible polymer obtained through the oxidative self-polymerization of dopamine under alkaline condition.[28–30] PDA exhibits excellent adhesive strength, high surface reactivity, and a capacity to conjugate with a wide range of biomolecules, including antibodies and aptamers.[31–33]

In this study, we report the fabrication of a novel PDA NPs-based electrochemical immunosensor for the sensitive and selective detection of cotinine. Unlike conventional methods that often require surface modification of nanoparticles prior to antibody attachment, our approach employs a direct conjugation strategy in which carboxyl groups of antibodies are activated using the coupling agents EDC/NHS, enabling covalent attachment to amine groups on PDA NPs. This mechanism is similar to a previous study that employed site-directed immobilization of protein A on amine-functionalized surfaces using EDC/sulfo-NHS chemistry to enhance antibody orientation and antigen-binding efficiency.[34] This simplified conjugation method not only reduces the number of processing steps but also helps maintain antibody bioactivity. These advantages are harnessed to construct a robust and efficient electrochemical sensing platform for cotinine, which holds significant potential for supporting smoking cessation programs, public health surveillance, and personalized medicine strategies.

2 Experimental details

2.1. Materials and apparatus

All chemicals and reagents were of analytical grade. Dopamine hydrochloride ($M_W = 189.64$) and Tris base ($M_W = 121.14$) were purchased from Sigma-Aldrich (St. Louis, USA) and Promega (Madison, USA), respectively. Mouse monoclonal anti-cotinine antibody (anti-COT Ab) was purchased from Abbexa biotechnology (Cambridge, UK). *N*-(3-Dimethylaminopropyl)-*N*′-ethyl carbodiimide hydrochloride (EDC) and *N*-hydroxy succinimide (NHS) were purchased from Sigma-Aldrich. (−)-Cotinine was purchased from Abcam (Cambridge, UK). (−)-Cotinine was prepared in methanol. Phosphate-buffered saline (PBS) at pH 7.4 was used as a diluent for working solution of cotinine concentrations and for all washing steps. Screen-printed carbon electrodes (SPCEs) were obtained from Quasense (Bangkok, Thailand). Electrochemical measurement, cyclic voltammetry (CV), electrochemical impedance spectroscopy (EIS), and differential pulse voltammetry (DPV) were conducted using a PalmSens4 potentiostat system (Palm Sens BV Co., Netherlands) with PS Trace 5.6 software and a three-electrode setup consisting of an Ag/AgCl reference, 2.5 mm carbon working, and carbon counter electrodes. The hydrodynamic diameter (*Z*-average) and polydispersity index (PDI) of PDA NPs and PDA NPs-conjugated antibodies (PDA NPs-Ab) were determined using a Zetasizer Nano ZS (Malvern Panalytical, Worcestershire, UK). The functional groups of PDA NPs, EDC/NHS-activated antibody (EDC/NHS-Ab), and PDA NPs-Ab were analyzed using a Bruker TENSOR II ATR-FTIR spectrometer (Bruker, Germany). A redox indicator solution was prepared with 5 mM potassium ferricyanide ($K_3[Fe(CN)_6]$) and 0.1 M potassium chloride (KCl) in PBS (1X, pH 7.4).

2.2. Synthesis of polydopamine nanoparticles

PDA NPs were synthesized through the self-oxidative polymerization of dopamine hydrochloride in an alkaline Tris buffer.[35] Specifically, 0.025 g of dopamine hydrochloride was dissolved in 50 mL of 10 mM Tris buffer (pH 10.5) and stirred gently at room temperature (RT) for 20 hours using a magnetic stirrer. Following polymerization, the PDA solution was isolated by centrifugation at 16 100×*g* for 5 min, then washed twice with Tris buffer. Finally, the obtained PDA NPs were resuspended in 100 μL of Tris buffer.

2.3. Fabrication of electrochemical immunosensor

Equal volumes (20 μL) of EDC–NHS (100 μM, 1 : 1) and anti-COT Ab (80 μg mL^{-1}) were incubated at RT for 120 min to activate the antibody's carboxyl groups. After activation, 60 μL of PDA NPs were added to the anti-COT Ab solution and allowed to conjugate for 30 min. The PDA NPs-Ab conjugates were washed twice with PBS to remove unbound components. In this process, the carboxyl groups of the antibodies were activated by EDC–NHS coupling and subsequently reacted with the amine groups on the PDA surface to form stable amide bonds ensuring strong attachment and selective cotinine recognition.[36] Subsequently, 7 μL of the conjugates were applied to the working electrode surface *via* drop-coating and incubated at RT for 60 min. The electrode was then rinsed, dried, and stored at 25 °C for later use.

2.4. Optimization of experimental parameters

To optimize sensor performance, five parameters including antibody activation time, antibody concentration, immobilization time, antigen incubation time, and the effect of pH on cotinine detection were systematically varied and evaluated using a DPV technique. The antibody was activated with EDC/NHS (100 μM, 1 : 1) for different durations (30–120 min) before conjugation with PDA NPs. Various antibody concentrations (20–120 μg mL^{-1}) were tested under the optimized activation condition. Immobilization time between the activated antibody and PDA NPs was varied (30–120 min) to determine the optimal conjugation efficiency. The fabricated PDA NPs-Ab/SPCE electrodes were then incubated with

cotinine antigen for different durations (30–120 min) at various pH values (3.0–9.0) to evaluate binding efficiency. DPV responses were recorded in 5 mM $[Fe(CN)_6]^{3-/4-}$ containing 0.1 M KCl after each optimization step.

2.5. Electrochemical response

For electrode characterization, CV and EIS were performed after each surface modification. CV was conducted from −0.6 V to 0.9 V at a scan rate of 0.1 V s^{-1}. EIS was recorded at the open-circuit potential over a frequency range of 10^{-1} to 10^{5} Hz. For target binding, 7 μL of the cotinine sample was applied to the modified electrode and incubated at RT for 90 min. After incubation, the electrode was rinsed with PBS to remove any unbound molecules. For target detection, DPV measurement was carried out from −0.015 V to 0.6 V with a pulse amplitude of 100 mV and a pulse period of 0.2 s. All measurements were performed using 5 mM $[Fe(CN)_6]^{3-/4-}$ at a ratio of 1 : 1 (v/v) with 1 M KCl in PBS (1X, pH 7.4). The change in peak current (ΔI) was calculated as the absolute difference between the peak current of the baseline measurement (I_0), obtained in the absence of the target analyte, from the peak current obtained after target addition (I), using the equation $\Delta I = I_0 - I$. A schematic of the proposed electrochemical immunosensor is shown in Scheme 1.

2.6. Analytical recovery assay

Urine samples were collected in containers with polyethylene screw caps. The optimal dilution for sample analysis was determined by monitoring ΔI *via* DPV. Cotinine concentrations (100 and 1000 ng mL^{-1}) were spiked into normal human urine samples, which were diluted 1 : 100 with PBS buffer. The % recovery was calculated using the formula:

$$\%\ \text{Recovery} = \frac{(\text{spiked sample result} - \text{unspiked sample result})}{\text{known add spiked concentration}} \times 100$$

Precision was assessed by calculating the relative standard deviation (RSD%):

$$\text{RSD}\% = \frac{\text{SD}}{x} \times 100$$

where SD is the standard deviation, and x is the mean of the measurements.

2.7. Specificity of the developed electrochemical immunosensor

Interfering substances, including 5 mg mL^{-1} of urea, sodium chloride, glucose, ascorbic acid, and 100 ng mL^{-1} of haemoglobin and albumin, were tested against a known cotinine concentration (100 ng mL^{-1}). DPV was used to measure the responses and evaluate the effect of these interferents on the cotinine signal.

2.8. Stability of the developed electrochemical immunosensor

The storage stability of the PDA NPs-based biosensor was evaluated over six weeks at RT (25 °C). The relative current

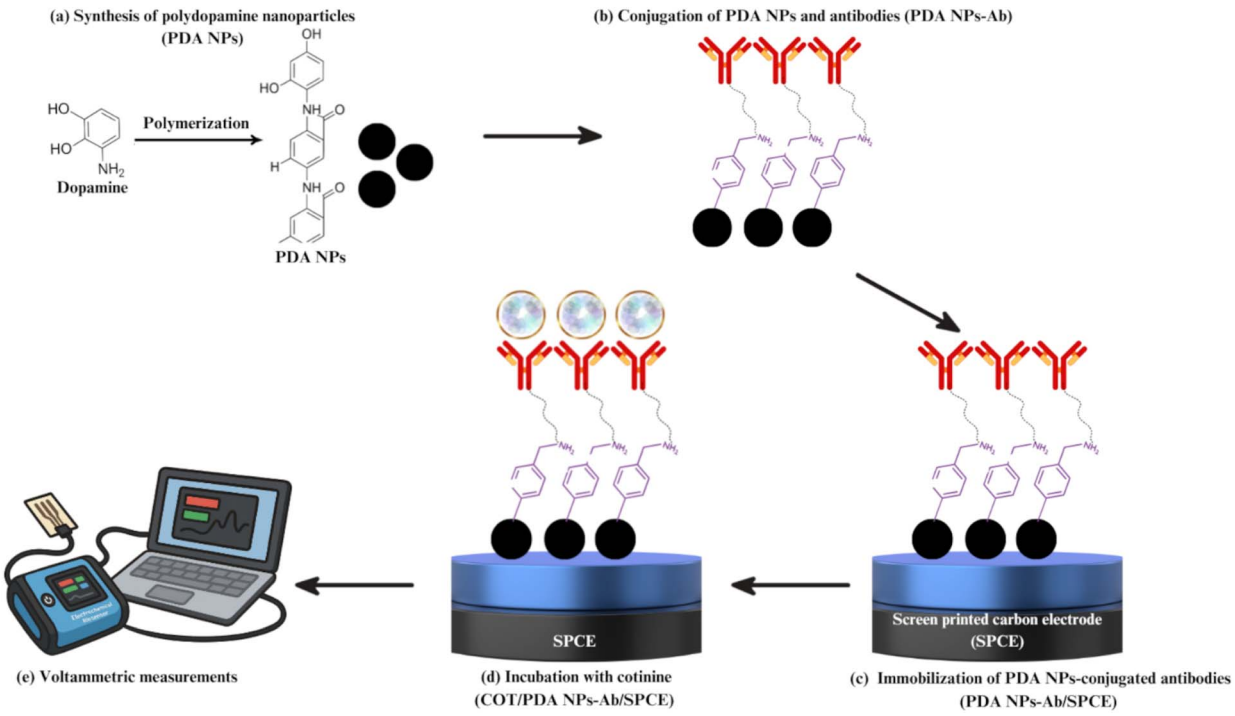

Scheme 1 Schematic illustration of the fabrication and detection process of the PDA NP-based cotinine immunosensor. (a) Synthesis of PDA NPs *via* dopamine polymerization, (b) covalent conjugation of PDA NPs with anti-COT Ab using EDC–NHS chemistry, (c) immobilization of PDA NPs-Ab conjugates on SPCE, (d) specific binding of cotinine to PDA NPs-Ab/SPCE, (e) electrochemical detection of cotinine using voltametric measurements.

response (%) was measured weekly using DPV and compared with the initial response at week 0. Triplicate measurements were performed each week using a cotinine concentration of 100 ng mL^{-1} to ensure consistency and reliability of the results.

2.9. Characterization techniques of PDA NPs and PDA NPs-Ab

2.9.1. Dynamic light scattering (DLS). The size and zeta potential of PDA NPs and PDA NPs-Ab were measured using a Zetasizer Nano system (Malvern, UK). Bare PDA NPs and PDA NPs-Ab were diluted in 1X PBS to the same concentration. A 1.0 mL aliquot of each diluted sample was placed into a disposable polystyrene cuvette and analyzed at 25 °C using the viscosity and refractive index of water. Each sample was measured in triplicate for 30 s, and results are presented as number average ± SD for particle size and PDI.

2.9.2. Fourier transform infrared (FTIR) spectra. FTIR analysis was conducted to investigate the functional groups and confirm the chemical modifications of each sample. Spectra were collected for Ab, EDC/NHS-Ab, bare PDA NPs, and PDA NPs-Ab. Measurements were performed using a Bruker TENSOR II spectrometer equipped with an attenuated total reflectance (ATR) accessory. Five microliters of each sample were placed directly onto the ATR crystal as a liquid drop and air-dried for 10 min to eliminate H_2O spectral interference. The spectral range was set from 4000 to 500 cm^{-1}, with a resolution of 4 cm^{-1} and 32 scans per sample to ensure sufficient signal quality. The ATR crystal was cleaned with DI water and ethanol to prevent cross-contamination. All spectra were processed using Bruker OPUS software for baseline correction and normalization prior to analysis.

3 Results and discussion

3.1. DLS analysis

As shown in Table 1, DLS analysis revealed a narrow size distribution of PDA NPs, with a *Z*-average diameter of 181.27 ± 1.61 nm and a low PDI of 0.10 ± 0.03. Upon conjugation with antibodies, the average size increased significantly to 708.50 ± 90.23 nm, and the PDI rose to 0.48 ± 0.06. These findings confirm the successful conjugation of antibodies to PDA NPs. Notably, a PDI value greater than 0.4 has been reported for nanoparticle-antibody conjugates, indicating a broad size distribution, which is considered acceptable in a similar study.[37] This substantial increase in particle size reflects successful surface modification of the PDA NPs through antibody conjugation.

3.2. FTIR analysis

Fig. 1a shows the FTIR spectra of the pure Ab (black line) and the EDC/NHS-Ab (red line). Both spectra exhibited characteristic peaks at 1636 cm^{-1} (amide I), 1545 cm^{-1} (amide II), 3070 cm^{-1} (N–H stretching), and 1080 cm^{-1} (PO_2^- symmetric stretching) in the protein backbone, confirming the antibody's protein structure.[38–40] After activation with EDC/NHS, a zero-length cross-linker that forms covalent bonds without spacer atoms, the antibody showed reduced band intensities indicating chemical modification of functional groups but no significant changes to its overall structure.[41] The FTIR spectra of bare PDA NPs (orange line) and PDA NPs-Ab (green line) are depicted in Fig. 1b. The bare PDA NPs exhibited characteristic peaks at 3348 cm^{-1} (O–H stretching), 2943 cm^{-1} (C–H stretching), 1587 and 1465 cm^{-1} (C=C stretching), consistent with the structure of polydopamine.[42,43] Upon conjugation with the antibody, new peaks emerged at 1603 and 1285 cm^{-1} (amide I and III bands).[44,45] The appearance of these amide bands directly confirms the successful attachment of the antibody

Table 1 DLS measurements

Sample	*Z*-average size (nm)	PDI
PDA NPs	181.27 ± 1.61	0.10 ± 0.03
PDA NPs-Ab	708.50 ± 90.23	0.48 ± 0.06

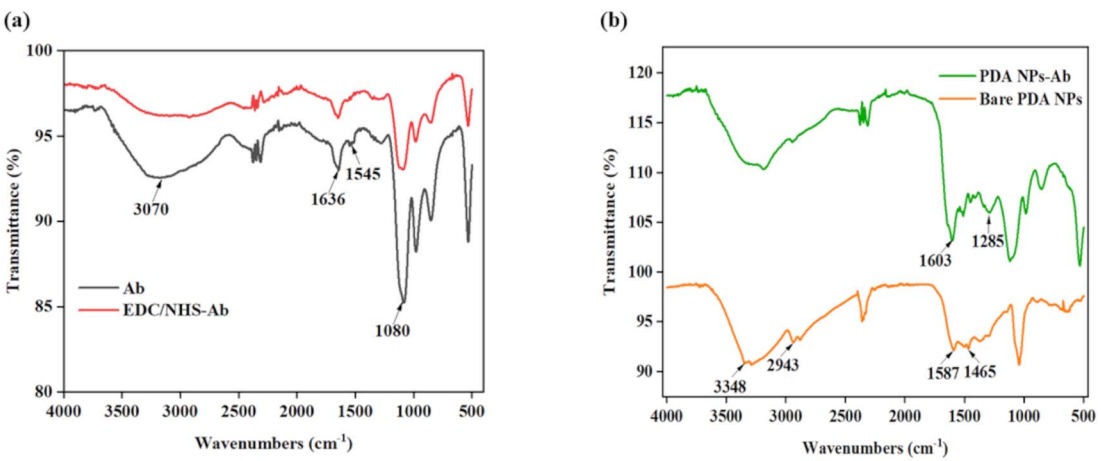

Fig. 1 FTIR spectra of (a) Ab and EDC/NHS-Ab, and (b) bare PDA NPs and PDA NPs-Ab.

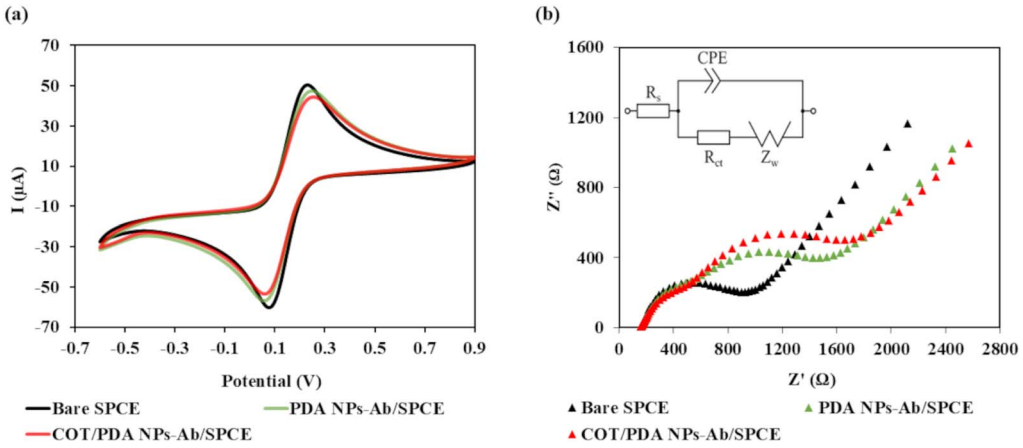

Fig. 2 Electrochemical characterization of the cotinine immunosensor: (a) CV and (b) EIS of bare SPCE, PDA NPs-Ab/SPCE, and COT/PDA NPs-Ab/SPCE in 5 mM $[Fe(CN)_6]^{3-/4-}$ with 0.1 M KCl.

onto the PDA surface, indicating successful functionalization *via* EDC/NHS-mediated coupling.

3.3. Electrochemical characterization of cotinine immunosensor

The electrochemical performance of the fabricated cotinine immunosensor was characterized using CV and EIS, as illustrated in Fig. 2. CV measurements were performed at a scan rate of 0.1 V s^{-1}. In the CV analysis (Fig. 2a), the bare SPCE exhibited the highest redox peak currents, indicating efficient electron transfer at the electrode surface. Upon modification with PDA NPs-conjugated antibodies (PDA NPs-Ab/SPCE), a notable decrease in peak current (I_p) was observed, attributed to the insulating properties of the biomolecular layer. Further suppression of redox peaks occurred after the introduction of cotinine (COT/PDA NPs-Ab/SPCE), confirming successful antigen–antibody interaction and the formation of an insulating immunocomplex on the electrode surface. In the equivalent circuit model used to describe the electrochemical impedance behaviour of the sensor, R_s represents the solution resistance, reflecting the ionic conductivity of the electrolyte; R_{ct} denotes the charge transfer resistance corresponding to the electron transfer kinetics at the electrode interface; Z_w corresponds to the Warburg impedance, indicating diffusion-limited processes at the electrode interface; and CPE (constant phase element) accounts for non-ideal capacitive behaviour arising from surface heterogeneity. As shown in (Fig. 2b), the Nyquist plots reveal a progressive increase in R_{ct} from the bare SPCE to PDA NPs-Ab/SPCE and further to COT/PDA NPs-Ab/SPCE. This trend confirms the successful stepwise modification of the electrode surface, reflecting the increasing barrier to electron transfer caused by the insulating nature of the polydopamine, antibodies, and the antigen–antibody complex. Although the differences in I_p appeared small, they showed a consistent decreasing trend across the modification steps, which is

Table 2 Summary of I_p and R_{ct} for various electrode modifications

Electrodes	I_p (μA)	R_{ct} (Ω)
Bare SPCE	59.69	569.73
PDA NPs-Ab/SPCE	56.09	626.50
COT/PDA NPs-Ab/SPCE	53.29	667.30

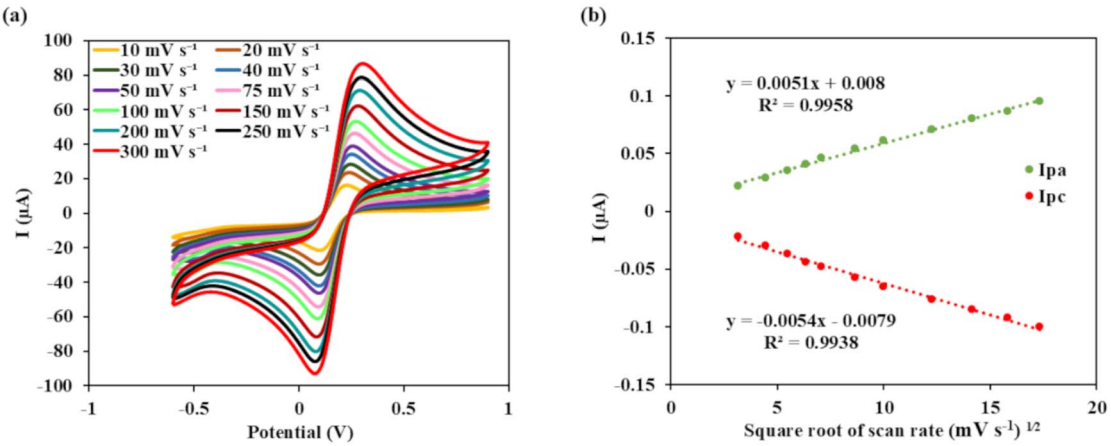

Fig. 3 Scan rate study of the PDA NPs-modified cotinine immunosensor: (a) CV at different scan rates (10–300 mV s^{-1}) and (b) Randles–Sevcik plot of anodic and cathodic peak current *vs.* square root of scan rate.

supported by a corresponding increase in R_{ct} in the EIS data (summarized in Table 2). The lower I_p and higher R_{ct} observed at the final COT/PDA NPs-Ab/SPCE stage reflected successful antibody-cotinine interactions that partially impeded electron transfer and decreased peak current. In the EIS spectra, the appearance of two semicircular portions for PDA NPs-Ab- and COT-modified electrodes suggests the presence of two distinct electrochemical processes occurring at the electrode interface. This phenomenon has been reported in a previous study and is often attributed to the formation of complex interfacial architectures, such as multi-layered films, heterogeneous surface coverage, or dual charge-transfer pathways resulting from biomolecule immobilization and target binding.[46] Therefore, the combined CV and EIS results provide reliable evidence of sensor responsiveness for cotinine detection.

3.4. Scan rate study

The effect of scan rate on the electrochemical response of the cotinine immunosensor was examined using CV in the range of 10 to 300 mV s^{-1}. As shown in Fig. 3a, both anodic and cathodic peak currents increased progressively with scan rate, while peak potential shifted slightly, which is characteristic of systems with diffusion-controlled electron transfer.[47] To further evaluate the reaction kinetics, peak currents were plotted against the square root of the scan rate, as illustrated in Fig. 3b. The resulting linear relationships for both the anodic (I_{pa}) and cathodic (I_{pc}) peak currents *versus* the square root of the scan rate ($R^2 = 0.9958$ and 0.9938, respectively), along with slope values close to 0.5, confirm that the redox process is diffusion-controlled rather than adsorption-controlled.[48] These findings confirm that the developed immunosensor operates *via* a diffusion-controlled mechanism, aligning with classical electrochemical behaviour described by the Randles–Sevcik model.[49] The electroactive area of the bare SPCE (6.3×10^{-7} cm^2) slightly decreased to 5.3×10^{-7} cm^2 after PDA NPs-Ab conjugation, calculated using the Randles–Sevcik equation with 5 mM $[Fe(CN)_6]^{3-/4-}$.[50] This minor decrease indicates partial surface coverage by biomolecules while retaining sufficient electroactive sites for efficient electron transfer, confirming successful immobilization.

3.5. Parameter optimization

To enhance the biosensor performance, five critical parameters were optimized using DPV measurements. As shown in Fig. 4a, the increase of the activation time of the antibody with EDC/NHS from 30 to 120 min significantly improved ΔI, with the highest signal observed at 120 min. The extended activation time enhances the efficiency of carbodiimide-mediated coupling by promoting the formation of stable NHS esters through the intermediate *O*-acylisourea, which is initially formed when EDC reacts with surface carboxyl groups. Consistent with a previous study, longer reaction duration (over 20 min) increased the number of activated sites available for covalent reaction with primary amine groups on the PDA NPs surface, promoting greater antibody immobilization and stronger signal responses.[51] Fig. 4b illustrates the effect of varying antibody concentrations. ΔI increased with concentration, the highest peak at 80 μg mL^{-1}. Higher concentrations at 120 μg mL^{-1} showed a slight decrease, likely due to steric hindrance and oversaturation on the electrode surface, reducing electron transfer efficiency. This observation aligns with a previous study demonstrating that increased surface coverage can lead to steric crowding, hindering efficient electron transfer.[52] The optimal immobilization time was 60 min (see Fig. 4c). Beyond 60 min, the signal plateaued, suggesting that sufficient immobilization had occurred, and and further extension did not enhance sensor performance. As shown in Fig. 4d, ΔI increased with incubation time, reaching a maximum at 90 min. Prolonged incubation beyond this point did not enhance the signal further, indicating that antibody-analyte binding reached equilibrium at 90 min. The

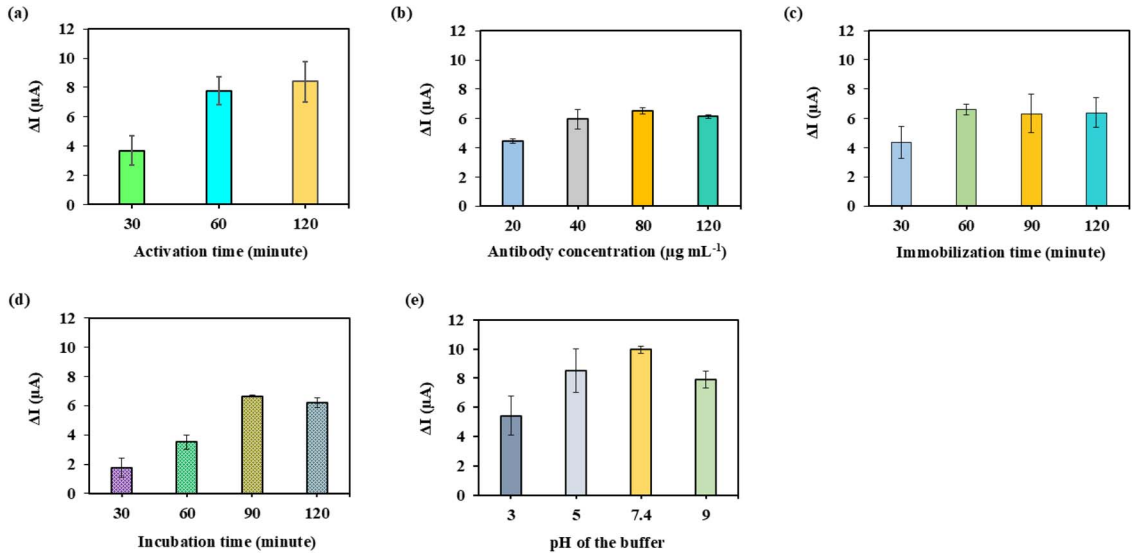

Fig. 4 Optimization of the biosensor with different parameters: (a) activation time of the antibody with EDC/NHS, (b) effect of antibody concentrations, (c) immobilization time of PDA NPs-Ab conjugates, (d) incubation time with cotinine, and (e) influence of pH buffer solution.

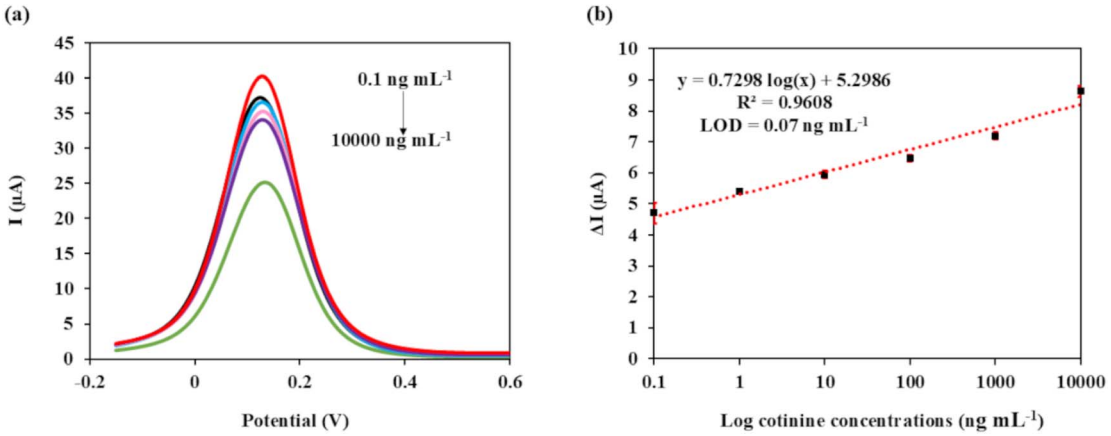

Fig. 5 (a) DPV responses of the PDA NPs-Ab/SPCE for cotinine from 0.1 to 10000 ng mL^{-1}, and (b) corresponding calibration curve of the electrochemical immunosensor for cotinine detection.

application of an immunosensor to detect cotinine in urine samples is expected to be affected by the pH of urine (Fig. 4e). ΔI increased from pH 3.0 to 7.4, reaching a maximum at 7.4, and decreased with alkalinization, because extreme pH can denature proteins.[53] Thus, pH 7.4 was selected as optimal, ensuring antigen stability and antibody activity. These optimized parameters were selected for subsequent sensor fabrication to ensure maximum sensitivity.

3.6. Electrochemical detection of cotinine

The electrochemical immunosensor exhibited a concentration-dependent response to cotinine, as evidenced by a gradual decrease of the anodic peak current in DPV measurements with increasing cotinine concentration (Fig. 5a). The linear relationship ($R^2 = 0.9608$) observed in the calibration plot (Fig. 5b) between ΔI and the logarithm of cotinine concentrations (0.1 to 10 000 ng mL^{-1}) confirms the sensor's quantitative capability. The limit of detection (LOD) was calculated based on the SD of the blank signal and the slope of the calibration curve using the formula: LOD = (3 × SD of blank)/slope. The calculated LOD of 0.07 ng mL^{-1} suggests a competent analytical sensitivity for cotinine detection using this electrochemical approach, which is sufficient to detect cotinine in passive smokers.[54,55] To contextualize the performance of the developed biosensor, Table 3 summarizes and compares the LODs and linear sensing ranges of various previously reported methods for cotinine detection.[11,56–61] The enhancement of the sensitivity of the PDA NPs-based immunosensor compared to previous studies is due to optimization conditions including EDC–NHS activation, antibody concentration, immobilization time, and incubation time with cotinine, which ensured stable and efficient antibody binding on the PDA surface. These results highlight the competitive sensitivity and broad dynamic range of this platform, supporting its potential applicability in clinical and POCT settings. Although PDA NPs were used in this study, future work could explore nanomaterials such as ZnO, TiO_2, and Fe_3O_4 to enhance sensor performance. ZnO offers high electron mobility, TiO_2 provides chemical stability, Fe_3O_4 enables magnetic separation, though aggregation and cytotoxicity should be addressed.[66–68]

3.7. Specificity analysis

The specificity of the immunosensor was evaluated by assessing the relative cross-reactivity towards potential interfering substances (5 mg mL^{-1} of urea, sodium chloride, glucose, ascorbic acid, and 100 ng mL^{-1} of haemoglobin and albumin) at concentrations significantly higher than the target analyte (cotinine, 100 ng mL^{-1}). As depicted in Fig. 6, the immunosensor exhibited negligible or low cross-reactivity (<30%) towards all tested interferents compared to cotinine, indicating

Table 3 Comparison of LOD and linear sensing range of various detection methods for cotinine

Method	LOD (ng mL^{-1})	Linear sensing range (ng mL^{-1})	Sample	Ref.
High-performance liquid chromatography	30	100–10000	Urine	11
Gas chromatography mass spectrometry	20	100–5000	Urine	56
Enzyme modified electrochemical immunochromatography	189.7	0–1000	Urine	57
Immunochromatographic sensor	1	1–100	Serum	58
Molecularly imprinted solid-phase extraction	10	30–500	Saliva	59
Impedimetric magneto-biosensor	0.000579	0.002–0.3	Serum, saliva	60
Boron-doped diamond electrode-based biosensor	10.7	0.08917–17.833	Saliva	61
PDA NPs-modified electrochemical cotinine immunosensor	0.07	0.1–10000	Urine	This work

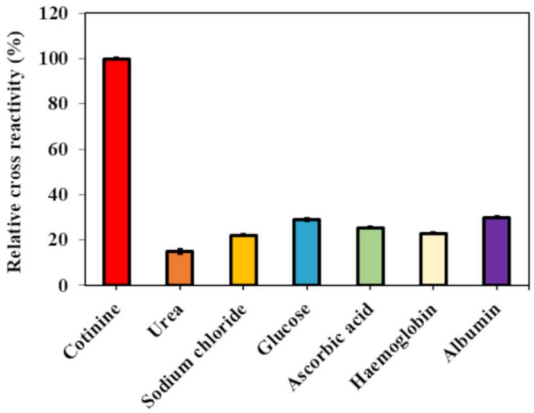

Fig. 6 Specificity test of the PDA NPs-modified cotinine immunosensor tested against common interferents using DPV.

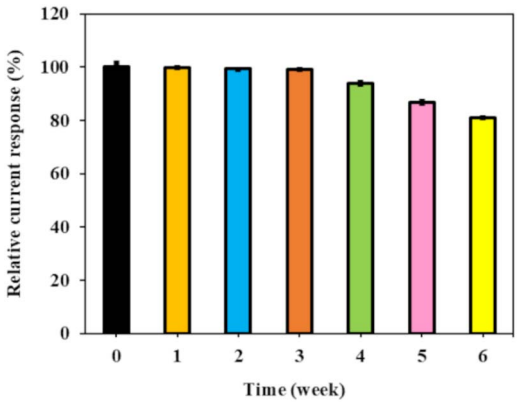

Fig. 8 Relative current response (%) of the PDA NPs-modified cotinine immunosensor over 6 weeks of storage at 25 °C.

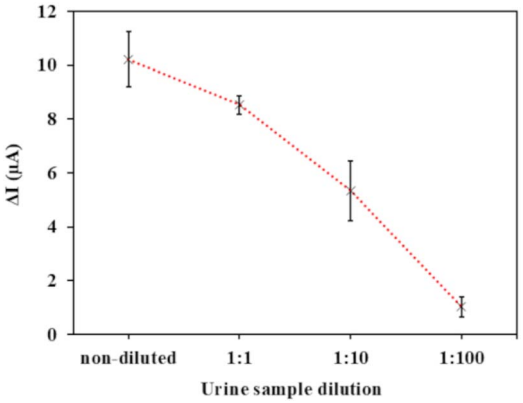

Fig. 7 Optimization of urine sample dilution with PBS (1X, pH 7.4).

a high degree of specificity to detect cotinine and minimal susceptibility to common biological matrix components. The high specificity of the PDA NPs-based immunosensor arises from the dual action of the anti-cotinine antibody and PDA NPs, which may be due to both primary immunological recognition and the antifouling property of PDA surface, whose biocompatible, dense coating minimizes nonspecific adsorption. This combination enhanced binding specificity and maintained stable electrochemical signals in complex biological matrices, consistent with a previous report on PDA surfaces.[62]

3.8. Recovery analysis

To validate the analytical reliability of the developed cotinine immunosensor in a complex biological matrix, a spike recovery assay was performed using diluted human urine samples. The optimal dilution factor for sample analysis was determined to be 1 : 100 (urine:PBS), based on DPV measurements shown in Fig. 7, which demonstrated stable and distinguishable current responses while minimizing matrix effects. Cotinine was spiked into the diluted urine at two concentration levels: 100 and 1000 ng mL^{-1}, and the results of the recovery assay are summarized in Table 4. The immunosensor exhibited acceptable recovery rates and low relative standard deviation (RSD) values across replicates, aligning with established analytical guidelines that consider RSD values below 3.3% as indicative of good precision and reproducibility.[63] These results demonstrate that the immunosensor provides reliable and reproducible detection of cotinine in urine, and a 1 : 100 urine dilution effectively reduces matrix interference while maintaining assay sensitivity.

3.9. Stability test

Storage stability of the developed immunosensor based on PDA NPs was evaluated over six weeks at RT (25 °C), which was chosen to reflect practical storage conditions. As shown in Fig. 8, the immunosensor maintained over 99% of its initial current response during the first three weeks, indicating good short-term stability. However, a gradual decline was observed thereafter, with the sensor retaining only 81.0% of its initial response by week 6. This decrease may be attributed to biomolecule degradation over time, highlighting a limitation in the long-term stability of the biosensor under ambient storage conditions. A previous study reported that PDA-coated biomaterials retained approximately 71.4% of their initial activity after 90 days at RT, highlighting the role of PDA coating in

Table 4 Recovery assay for cotinine detection in spiked urine samples

Cotinine concentrations spiked in urine sample (ng mL^{-1})	Measured concentration (ng mL^{-1})	Recovery (%)	RSD (%) ($n = 3$)
100	132.74 ± 0.02	132.74	0.43
1000	1047.13 ± 0.13	104.71	3.17

maintaining stability under ambient conditions.[64] Compared to a previous study using bovine serum albumin (BSA)-coated magnetic Fe_3O_4 nanoparticles stored at 4 °C, which reported 77.8% sensitivity retention after six weeks, the PDA NPs-based immunosensor showed comparable stability under less controlled storage conditions.[65] These findings support the feasibility of PDA NPs as stable bioplatforms, while also highlighting the importance of optimizing storage environments for long-term applications.

4 Conclusions

This study presents a sensitive and selective electrochemical immunosensor for cotinine detection, utilizing PDA NPs for the efficient antibody immobilization. FTIR analysis confirmed successful bioconjugation through the presence of amide band signatures, while electrochemical characterization (CV and EIS) validated stepwise electrode modification and antigen–antibody interaction. The sensor demonstrated a wide linear range (0.1–10 000 ng mL^{-1}) and a LOD (0.07 ng mL^{-1}), determined by DPV. CV analysis confirmed that the sensor exhibited diffusion-controlled electrochemical behaviour. High specificity and accurate recovery in diluted urine samples highlight the immunosensor's reliability in complex matrices. Additionally, the sensor maintained over 80% of its original signal after six weeks of storage at RT, indicating good operational stability. The novelty of this study is the use of PDA NPs for direct antibody immobilization *via* EDC/NHS coupling, which preserved antibody activity and minimized nonspecific adsorption for selective and stable cotinine detection. Overall, this PDA-based platform offers a promising approach for POCT cotinine monitoring and can be extended to the detection of other small-molecule biomarkers. For future work, system-level optimization using undiluted and varied biological fluids is essential to ensure robustness in clinical settings. Expanding the platform toward wearable formats and exploring multiplexing capabilities for simultaneous detection of other tobacco-related or health-relevant biomarkers could further broaden its applicability in preventive and personalized healthcare.

Ethical statement

The study was conducted in accordance with the Declaration of Helsinki and Clinical investigation of medical devices for human subjects – Good Clinical Practice, and the protocol was reviewed and approved by the Khon Kaen University Ethics Committee (HE674015). Informed consents were obtained from human participants of this study.

Author contributions

O. Z.: writing – original draft, methodology, investigation, formal analysis, conceptualization, data curation. N. N. S. A. and J. D.: writing – review & editing, funding acquisition. P. T.: writing – review & editing, supervision. P. C.: writing – review & editing. C. S., N. J., and P. C.: writing – review & editing. P. M.: writing – review & editing, writing – original draft, methodology, funding acquisition, conceptualization.

Conflicts of interest

The authors declare that they have no conflicts of interest.

Data availability

All data required to support the findings of this study are contained within the article. The data that support the findings of this study are available from the corresponding author upon reasonable request.

Acknowledgements

This research was supported by the Fundamental Fund of Khon Kaen University, the National Science, Research, and Innovation Fund (NSRF). The authors gratefully acknowledge the support received from the Centre of Research and Development of Medical Diagnostic Laboratories (CMDL), Faculty of Associated Medical Sciences, Khon Kaen University. This manuscript has been read and edited by Prof. Yukifumi Nawa, Dept of Tropical Medicine, Khon Kaen University *via* KKU Publication Clinic.

References

1 World Health Organization, *WHO Report on the Global Tobacco Epidemic 2023*, World Health Organization, Geneva, 2023, vol. 216.
2 J. Thakur, R. Garg, J. Narain and N. Menabde, *Indian J. Publ. Health*, 2011, **55**, 155.
3 K. Chang, S. Yang, S. Kim, K. Han, S. Park and J. Shin, *Int. J. Mol. Sci.*, 2014, **15**, 22279–22295.
4 A. Kulkarni and S. Banait, *Cureus*, 2023, **15**(10), e47779.
5 Z. Khan, J. Tönnies and S. Müller, *J. Cancer Epidemiol.*, 2014, **2014**, 394696.
6 A. Brown and S. J. Balk, *Curr. Probl. Pediatr. Adolesc. Health Care*, 2020, **50**, 100761.
7 A. G. O. Fernandes, L. N. Santos, G. P. Pinheiro, D. da Silva Vasconcellos, S. T. de Oliva, B. J. D. Fernandes and R. D. Couto, *Open Biomark. J.*, 2020, **10**, 60–68.
8 X. Tan, K. Vrana and Z.-M. Ding, *Front. Behav. Neurosci.*, 2021, **15**, 758252.
9 S. Kim, *Int. J. Environ. Res. Publ. Health*, 2016, **13**, 1236.
10 K. Parate, C. Karunakaran and J. C. Claussen, *Sens. Actuators, B*, 2019, **287**, 165–172.
11 Y.-H. Wen, P.-S. Yang and S.-S. Wu, *J. Food Drug Anal.*, 2009, **17**, 357–362.
12 M. Raja, P. Yadav, K. Jha and S. Handa, *J. Clin. Diagn. Res.*, 2016, **10**, ZE04–ZE06.
13 C. N. Man, L.-H. Gam, S. Ismail, R. Lajis and R. Awang, *J. Chromatogr., B: Anal. Technol. Biomed. Life Sci.*, 2006, **844**, 322–327.
14 A. Okayama and T. Sato, *Ind. Health*, 2004, **42**, 348–351.

15 T. Wielkoszyński, K. Tyrpień and M. Szumska, *J. Pharm. Biomed. Anal.*, 2009, **49**, 1256–1260.
16 E. T. S. G. da Silva, D. E. P. Souto, J. T. C. Barragan, J. d. F. Giarola, A. C. M. de Moraes and L. T. Kubota, *ChemElectroChem*, 2017, **4**, 778–794.
17 X. Jia, S. Dong and E. Wang, *Biosens. Bioelectron.*, 2016, **76**, 80–90.
18 J. Lee, O. Adegoke and E. Y. Park, *Biotechnol. J.*, 2019, **14**, e1800249.
19 M. Holzinger, A. Le Goff and S. Cosnier, *Front. Chem.*, 2014, **2**, 63.
20 S. L. Filbrun, A. B. Filbrun, F. L. Lovato, S. H. Oh, E. A. Driskell and J. D. Driskell, *Analyst*, 2017, **142**, 4456–4467.
21 S. Okyem, O. Awotunde, T. Ogunlusi, M. B. Riley and J. D. Driskell, *Bioconjug. Chem.*, 2021, **32**, 1753–1762.
22 R. Raghav and S. Srivastava, *Biosens. Bioelectron.*, 2016, **78**, 396–403.
23 S. Sanli, F. Ghorbani-Zamani, H. Moulahoum, Z. P. Gumus, H. Coskunol, D. Odaci Demirkol and S. Timur, *Anal. Chem.*, 2020, **92**, 1033–1040.
24 Y. Wu, C. Chen and S. Liu, *Anal. Chem.*, 2009, **81**, 1600–1607.
25 H. S. Hwang, J. W. Jeong, Y. A. Kim and M. Chang, *Micromachines*, 2020, **11**, 814.
26 S. Puertas, M. de Gracia Villa, E. Mendoza, C. Jiménez-Jorquera, J. M. de la Fuente, C. Fernández-Sánchez and V. Grazú, *Biosens. Bioelectron.*, 2013, **43**, 274–280.
27 H. Li, D. Yin, W. Li, Q. Tang, L. Zou and Q. Peng, *Colloids Surf. B Biointerfaces*, 2021, **199**, 111502.
28 T.-Y. Kuo and Y.-C. Chung, *Mater. Adv.*, 2021, **2**, 5686–5690.
29 H. Wu, C. Zhao, K. Lin and X. Wang, *Front. Bioeng. Biotechnol.*, 2022, **10**, 952500.
30 A. Aresta, S. R. Cicco, D. Vona, G. M. Farinola and C. Zambonin, *Separations*, 2022, **9**, 194.
31 I. S. Kwon and C. J. Bettinger, *J. Mater. Chem. B*, 2018, **6**, 6895–6903.
32 H. Feinberg and T. W. Hanks, *Polym. Int.*, 2022, **71**, 578–582.
33 J. H. Ryu, P. B. Messersmith and H. Lee, *ACS Appl. Mater. Interfaces*, 2018, **10**, 7523–7540.
34 Y.-S. Sohn and Y. K. Lee, *J. Biomed. Opt.*, 2014, **19**, 051209.
35 B. Poinard, S. Z. Y. Neo, E. L. L. Yeo, H. P. S. Heng, K. G. Neoh and J. C. Y. Kah, *ACS Appl. Mater. Interfaces*, 2018, **10**, 21125–21136.
36 H. Tumturk, F. Sahin and E. Turan, *Analyst*, 2014, **139**, 1093.
37 M. Conrad, G. Proll, E. Builes-Münden, A. Dietzel, S. Wagner and G. Gauglitz, *Microchim. Acta*, 2023, **190**, 62.
38 S. Islam, Moinuddin, A. R. Mir, A. Raghav, S. Habib, K. Alam and A. Ali, *J. Biomol. Struct. Dyn.*, 2018, **36**, 2637–2653.
39 S. Ahlawat, A. Nehra, V. Pandey and K. P. Singh, *Ionics*, 2019, **25**, 1887–1896.
40 D. Ami, P. Mereghetti, M. Leri, S. Giorgetti, A. Natalello, S. M. Doglia, M. Stefani and M. Bucciantini, *Sci. Rep.*, 2018, **8**, 12508.
41 J. Skopinska-Wisniewska, M. Tuszynska and E. Olewnik-Kruszkowska, *Materials*, 2021, **14**, 396.
42 P. Maraming, N. N. S. Aye, P. Boonsiri, S. Daduang, O. Buhome and J. Daduang, *Int. J. Mol. Sci.*, 2022, **23**, 13699.
43 J. Tan, Z. Xie, Z. Zhang, Y. Sun, W. Shi and D. Ge, *J. Mater. Sci.*, 2018, **53**, 447–455.
44 P. Klongklaew, P. Khamjapo, P. Sae-Oui, P. Jittham, S. Loykulnant and W. Intiya, *Polymers*, 2023, **15**, 3698.
45 K. H. Sizeland, K. A. Hofman, I. C. Hallett, D. E. Martin, J. Potgieter, N. M. Kirby, A. Hawley, S. T. Mudie, T. M. Ryan, R. G. Haverkamp and M. H. Cumming, *Materialia*, 2018, **3**, 90–96.
46 W. Yang, H. Ying, S. Zhang, R. Guo, J. Wang and W.-Q. Han, *Electrochim. Acta*, 2020, **337**, 135687.
47 K. J. Aoki, J. Chen, Y. Liu and B. Jia, *J. Electroanal. Chem.*, 2020, **856**, 113609.
48 K. Suliborska, M. Baranowska, A. Bartoszek, W. Chrzanowski and J. Namieśnik, *Proceedings*, 2019, **11**, 23.
49 O. A. González-Meza, E. R. Larios-Durán, A. Gutiérrez-Becerra, N. Casillas, J. I. Escalante and M. Bárcena-Soto, *J. Solid State Electrochem.*, 2019, **23**, 3123–3133.
50 P. Ranjan, M. Abubakar Sadique, S. Yadav and R. Khan, *ACS Appl. Mater. Interfaces*, 2022, **14**, 20802–20812.
51 V. G. Janolino and H. E. Swaisgood, *Biotechnol. Bioeng.*, 1982, **24**, 1069–1080.
52 S. Soleimani, T. A. Bruce-Tagoe, N. Ullah and M. K. Danquah, *Micromachines*, 2025, **16**, 162.
53 Y. Li, Y. Zhang, J. Han, P. K. Chu, J. Feng and Y. Dong, *RSC Adv.*, 2017, **7**, 2242–2248.
54 P. Sharma, N. Sane, S. Anand, P. Marimutthu and V. Benegal, *Indian J. Psychiatry*, 2019, **61**, 270.
55 P. Sathish Kumar, B. Shobana and P. Prakash, *Chemosphere*, 2024, **354**, 141708.
56 M. Iwai, T. Ogawa, H. Hattori, K. Zaitsu, A. Ishii, O. Suzuki and H. Seno, *Nagoya J. Med. Sci.*, 2013, **75**, 255–61.
57 N. Larpant, P. K. Kalambate, T. Ruzgas and W. Laiwattanapaisal, *Sensors*, 2021, **21**, 1659.
58 H. Nian, J. Wang, H. Wu, J.-G. Lo, K.-H. Chiu, J. G. Pounds and Y. Lin, *Anal. Chim. Acta*, 2012, **713**, 50–55.
59 R. V. Vitor, M. C. G. Martins, E. C. Figueiredo and I. Martins, *Anal. Bioanal. Chem.*, 2011, **400**, 2109–2117.
60 M. Aydın, E. B. Aydın and M. K. Sezgintürk, *Sens. Actuators, B*, 2024, **408**, 135476.
61 M. F. Alecrim, F. M. Oliveira, T. J. Guedes, C. D. c. Neves, V. A. Mendonça, E. S. Gil, R. M. Verly and W. T. P. dos Santos, *Electrochim. Acta*, 2016, **222**, 331–337.
62 D. Chen, Y. Mei, W. Hu and C. M. Li, *Talanta*, 2018, **182**, 470–475.
63 T. N. Rao, *Calibration and Validation of Analytical Methods – A Sampling of Current Approaches*, InTech, 2018.
64 H. Wang, W. Yue, S. Zhang, Y. Zhang, C. Li and W. Su, *Catalysts*, 2021, **11**, 1463.
65 M. Aydın, E. B. Aydın and M. K. Sezgintürk, *Sens. Actuators, B*, 2024, **408**, 135476.
66 M. L. M. Napi, S. M. Sultan, R. Ismail, K. W. How and M. K. Ahmad, *Materials*, 2019, **12**, 2985.
67 S. Nadzirah, S. C. B. Gopinath, M. Ammar, C. F. Dee, U. Hashim, A. R. Md Zain and B. Yeop Majlis, *Crit. Rev. Anal. Chem.*, 2025, 1–23.
68 M. D. Nguyen, H.-V. Tran, S. Xu and T. R. Lee, *Appl. Sci.*, 2021, **11**, 11301.